ГОДИШНИК НА СОФИЙСКИЯ УНИВЕРСИТЕТ „СВ. КЛИМЕНТ ОХРИДСКИ“
ФИЗИЧЕСКИ ФАКУЛТЕТ

Том 111

ANNUAL OF SOFIA UNIVERSITY “ST. KLIMENT OHRIDSKI”
FACULTY OF PHYSICS

Volume 111

TSUNAMI RADIATION PATTERN IN THE SOUTHERN AEGEAN SEA

LYUBA DIMOVA

Department of Meteorology and Geophysics

Люба Димова. РАЗПРОСТРАНЕНИЕ НА ВЪЛНИ ЦУНАМИ В ЮЖНАТА ЧАСТ НА ЕГЕЙСКО МОРЕ

В това изследване са представени различни сценарии на вълни цунами, генерирани от земетресения в южната част на Егейско море. Реконструирани са две от най-големите исторически събития на вълни цунами в цялото Средиземноморие. Допълнително са избрани и моделирани шест различни цунамигенни зони близо до островите Крит и Родос, за да се оценят максималните амплитуди и времето на пристигане на вълните цунами. За всички сценарии е моделиран правоъгълен сеизмичен източник, способен да генерира земетресение с магнитуд, равен или по-голям на регистрирания в исторически план магнитуд. Числено се моделират разпространението на вълните цунами, очакваните височини и ефектите по крайбрежните райони.

Lyuba Dimova. TSUNAMI RADIATION PATTERN IN THE SOUTHERN AEGEAN SEA

This paper presents several scenarios of earthquake-generated tsunami in the southern Aegean Sea. We reconstructed two of the largest historically known tsunami events in the area of the whole Mediterranean. Additionally we identified and modeled six different tsunamigenic zones near the islands of Crete and Rhodes to estimate the maximum water elevations and the arrival time of the tsunami. For all scenarios, we took into account rectangle seismic faults, capable to generate an earthquake with magnitude equal or slightly larger than the highest magnitude registered in historical times. Then we modeled numerically the tsunami wave propagation, the expected heights and some effects on the coastal areas.

Keywords: tsunami, numerical methods, earthquakes
PACS numbers: 91.30.Nw, 92.10.hl, 02.60.-x, 91.30.Px

For contact: Lyuba Dimova, Department of Meteorology and Geophysics, Faculty of Physics, Sofia University St. Kliment Ohridski,5, J. Bourchier Blvd., 1164 Sofia, Phone: +359 2 81 61 629, E-mail: lyuba_dimova@phys.uni-sofia.bg

1. INTRODUCTION

Mediterranean region suffered by numerous tsunamis in the past and many of them had catastrophic impact. Although tsunami catalogues are not complete enough regarding the early history events, the most of the tsunamis in the Mediterranean region are due to earthquakes. Some of the events are still with uncertain origin. Reconstruction of past historical events as well as hypothetical events in active seismic zones is important for the evaluation of the tsunami hazard in the region. In this study we focused on 8 tsunamigenic events in the southern Aegean Sea. Six of the tsunamigenic sources are located close to coast which is typical feature of the most sources in the Mediterranean. We took into account two more historical events that are quite important since the magnitude of both earthquakes is greater than 8. The impact of these strong events is comparable with the December 26, 2004 earthquake in Sumatra offshore. According to several catalogues and databases we built the hypothetical focal mechanism of 6 earthquakes, we calculated the geometry of the seismic faults and we reconstructed the tsunami waves referred to AD 21 July 365 event and AD 8 August 1303 event respectively for western Hellenic arc (WHA) and eastern Hellenic arc (EHA).

Aegean microplate is located in the eastern Mediterranean. Its southern boundary is the subduction zone south of Crete where the African plate submerged beneath the Aegean Sea plate. This area is among the most stressed part of the collision between the Eurasia and African plates therefore the seismicity there is the highest in the whole Mediterranean. The Hellenic arc parallels the subduction zone at a distance of about 120 km to the north. The Hellenic arc consists of two major transform faults, known as Cephalonia transform fault to the north-western ends and Rhodes transform fault to the eastern ends and several active volcanic points (Methana, Santorini, Nisyros, the Bodrum Peninsula). The seismicity along the Hellenic arc is extremely high with its shallow and intermediate depth of the earthquakes. The tsunamigenic potential of the earthquake sources is higher when the depth of the event is shallower. More than 4500 earthquakes (magnitude greater than 4.5) occurred in the area since the beginning of 20th century, while more than 100 events of tsunami waves present in the historical records since BC 1610 up to present. Fig. 1 shows earthquakes with magnitude greater than 4.5 and focal depth shallower than 100 km as well as historical tsunamigenic sources [1, 2].

2. TSUNAMIGENIC SOURCES

Eight potentially tsunamigenic seismic sources are selected in the region of southern Aegean Sea. As a major geotectonic structure, the Hellenic arc produces large earthquakes and tsunamis. Two of the key events in the region of Crete are discussed in the next sections. The location of both historical events is uncertain.

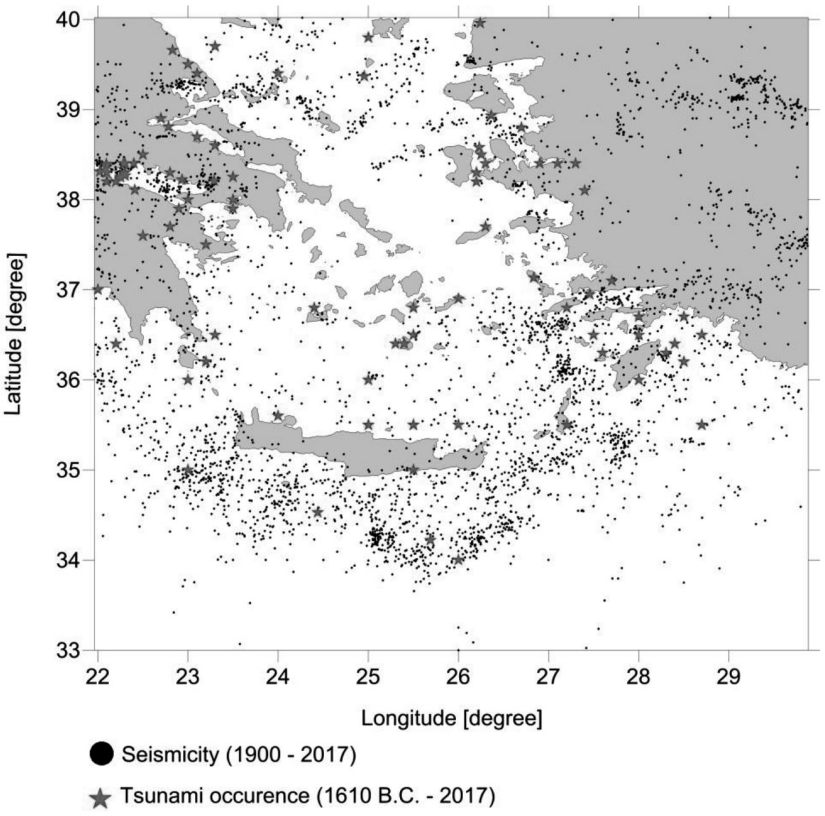

Fig. 1. Earthquake and tsunami occurrence in the southern Aegean Sea [1, 2]

It is considered that the large tsunamigenic earthquake occurred in AD 365 during the rupture of the western segment of the Hellenic subduction zone on a NE-dipping fault within the overriding plate [3]. This event destroyed cities and drowned thousands of people in the coastal regions from Alexandria (Egypt) to the Adriatic and Sicily. The moment magnitude M_w was estimated around ~8.3. The historical, geological and archaeological evidence leave little doubt that the tsunami in AD 365 was generated by 6–9 m co-seismic uplift in the area of West Hellenic Arc (WHA) [4].

The event from AD 1303 very likely occurred during the rupturing of the arc between Crete and Rhodes islands and it is one of the largest historically discoursed tsunamigenic earthquakes in the Mediterranean. The tsunami induced by the earthquake propagated long distances from Acre (Israel) through Alexandria (Egypt) and Libya. The most affected area was the north-eastern part of the coast of Crete and the capital Heraklion located to the north. The magnitude M_w is assumed to be around ~8.0. The tsunami intensity was reported to be X degree [4].

Many authors [e.g., 3, 5–8] simulated the large tsunamis of AD 365 and AD 1303 and the results show that the wave amplitudes are underestimated as compared to the ones expected from the historical and geological record of the tsunami. This may be due to rough bathymetry and inappropriate seismic source geometry.

Data for focal mechanisms and depth of the additional five tsunamigenic zones in the area of the southern Aegean Sea are taken into account utilizing the fault databases compiled in SHARE (The European Database of Seismogenic Faults), GreDaSS and DISS (The Database of Individual Seismogenic Sources) [9]. We simulated hypothetical earthquakes to estimate the tsunami impact for Crete and other small islands. Recent earthquake in the region of Gramvousa fault zone occurred in October 12, 2013 with $MW = 6.8$ without expecting any serious tsunami treat because of the depth of the earthquake. Yolsal and Taymaz [7] modelled several scenarios of tsunami waves generated by the earthquakes in the region of Ptolemy Trench. Karpathos Island was hit by tsunami, the eyewitness accounts the maximum tsunami run-up heights, associated with February 9, 1948 earthquake ($M \sim 7.0$) on the island of Karpathos, between 3.6– 7.0 m [10]. There are two main hypotheses on the origin of the tsunami- underwater earthquake or underwater landslide.

One more tsunamigenic zone that we studied in this work is located in the region of Rhodes. Since the seismicity there is high we chose one of the two earthquakes in 1957 with $M_w = 7.3$ and the corresponding focal mechanism [10], to explore possibility for tsunami and sequences on the nearest coasts. Fethiye town is one of the attractive tourist destinations in Turkey and was affected by earthquakes and tsunamis in the past [11].

The position of all eight tsunamigenic seismic faults is shown in Fig. 2. We took into account rectangle sources placed in different depths that respond to the upper border depth of the fault (UBDF). The proposed names of the seismic faults correspond to the databases cited before (SHARE, GreDaSS and DISS) and we named them as follow: WHA (AD 365), EHA (AD 1303), Gramvousa, Palaeochora-Tympaki, Ptolemy Trench, South Cretan Sea, Karpathos I and Rhodes.

The fault parameters of the selected sources are presented in Table 1. For each tsunamigenic zone we took into account an earthquake with magnitude equal to the largest magnitude registered in the past. The relation between the moment magnitude and the seismic moment, proposed by Hanks and Kanamori [12] is used to obtain the released energy. The seismic moment is related to the geometry of the faults and the slip on the faults by the regressions proposed in Mai and Beroza [13] and Wells and Coppersmith [14]. The longitude and latitude are converted in Universal Transverse Mercator (UTM) coordinate system since the calculations are made in Cartesian coordinates. The focal mechanisms for five of the tsunamigenic faults are selected to be in accordance with the database SHARE. Focal mechanisms for both of the reconstructed events and for Rhodes fault are taken in accordance with published data [10, 15–19].

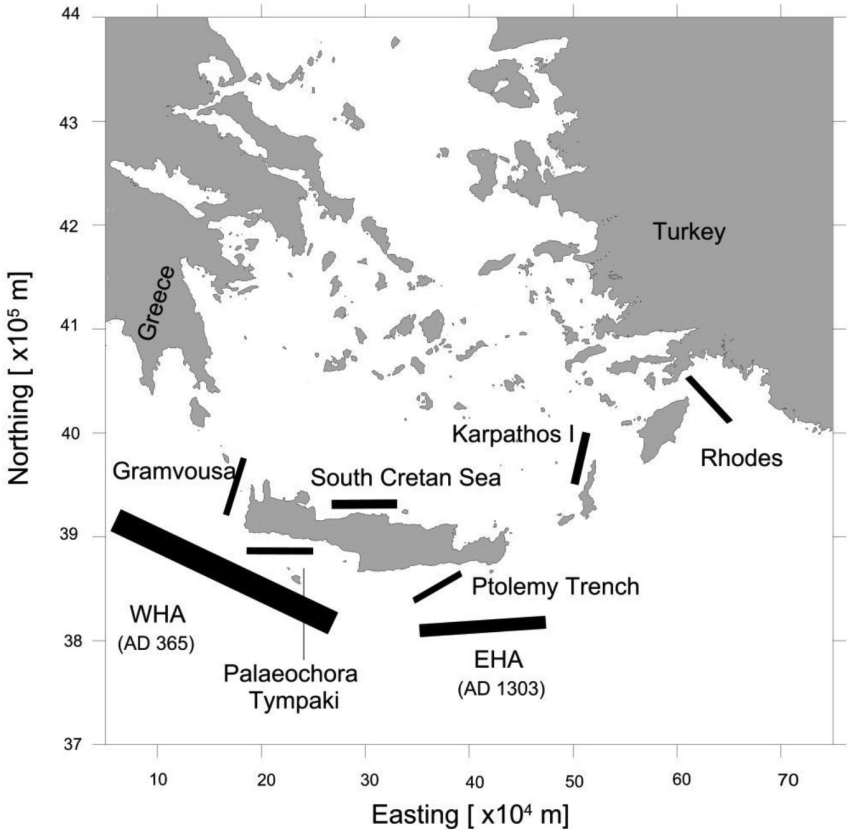

Fig. 2. Position of the tsunamigenic seismic sources

3. NUMERICAL MODELLING

The theory of numerical modelling of tsunami waves started its history during the last century but it is widely used after the 2004 tsunami in Sumatra where at least 230 000 people were killed. Numerical models are used to evaluate and predict the physical characteristics of tsunami. They play an important role in tsunami hazard mitigation and are especially useful for preparing maps of inundation for coastlines vulnerable to tsunami flooding. There are number of mathematical methods based on the resolution of bathymetry data and parameters of the seismic fault, developed to model and identify tsunami wave characteristics. Tsunami source models are well developed for submarine earthquakes, where the seafloor deformation is caused by a finite dislocation (i.e., slip on the fault) [20]. Simple implementation of this type of source model usually assumes a finite rupture interface with uniform dislocation (e.g., slip movement along a fault). We computed the initial conditions of studied events

implementing analytical formulas of Okada [20, 21] and appropriate bathymetry data. The basic parameters for each event described in Table 1 are essential for calculation of deformation of the sea bottom which specifies the initial tsunami waveform. Numerical code UBO-TSUFD is applied to model the propagation and the interaction of tsunami with the coastal areas. The code is developed in University of Bologna (Italy) and extensively used to study the propagation of tsunamis generated by earthquakes. We utilized this method since it was tested and validated for different benchmark problems based on analytical solutions: one on a plane wave propagating on a flat channel with a constant slope beach, and one on a laboratory experiment. Additionally it was proved for several realistic tsunami cases [22]. UBO-TSUFD reproduced quite well the theoretical and experimental data. The code solves the governing equations of Navier-Stocks in the shallow water theory approximation by using the finite-difference technique with an explicit leap-frog scheme on a staggered grid. Tsunami waves belong to the long-wave theory, therefore the vertical acceleration of water particles are negligible compared to the gravitational acceleration except for an oceanic propagation of tsunami [23]. A good approximation is that the pressure is hydrostatic and therefore the vertical motion of water particles has no effect on the pressure distribution. In addition the horizontal velocity of water particles are vertically uniform. There are several conditions that need to be fulfilled in order to have good results- initial conditions, boundary conditions, stability conditions, preparation of a grid and bathymetry data. Linear and nonlinear theories are used according to the degree of nonlinearity of the phenomena. Usually coarse grids in the deep ocean and fine grids in the nearshore zone are used. An expanded explanation of UBO-TSUFD can be found in [22, 23]. The code is extensively applied to simulate tsunami waves for seas like Mediterranean and other small basins, where the Coriolis force is neglected.

The code computes water surface oscillations, velocity field, arrival time of the waves and water inundation when nonlinearity is applied. The grid used in our calculations has cells with 500×500 m resolution. The utilized time step is 1.5 s and it is adjusted to satisfy the CFL (Courant-Friedrichs-Lewy) stability condition (1):

$$\frac{\Delta x}{\Delta t} = \sqrt{2gH}\,, \tag{1}$$

where Δx is the cell size, Δt is the time step for every cell, g is the gravity acceleration and H is the maximum depth of the ocean, in our case for the Mediterranean region it is 4500 m.

The total number of nodes of the grid is 2803401. The resolution of the bathymetry and topography data is 30 s [24]. Bathymetry map of the studied region is shown in Fig. 3.

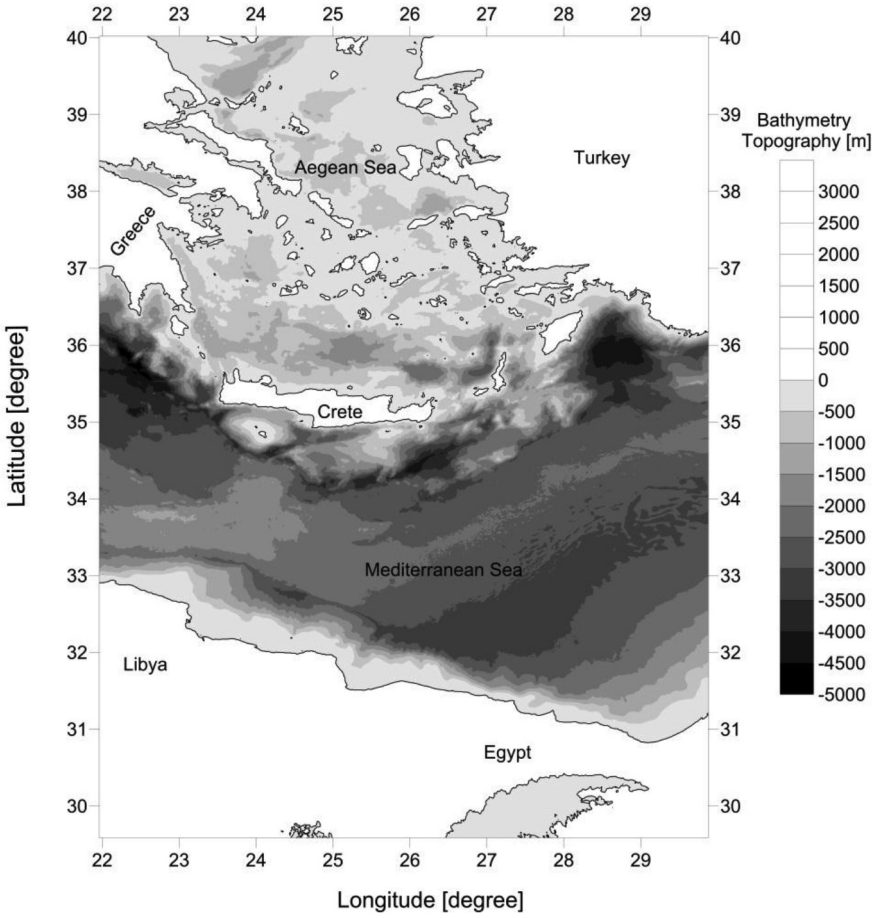

Fig. 3. Bathymetry map of the region

Table 1. Seismic fault parameters

Tsunamigenic zone	Position [lon, lat]	Magnitude Mw	UBDF* [km]	Length [km]	Width [km]	Slip [m]	Strike [degree]	Dip [degree]	Rake [degree]
WHA AD 365	23.0, 35.0	8.3	5	200	80	9	295	15	90
EHA AD 1303	26.1, 34.5	8.0	4	125	50	6	268	48	71
Gramvousa	23.5, 35.5	6.8	2	25	14	2	180	80	270
Palaeochora-Tympaki	24.0, 35.2	7.0	2	33	15	2.5	100	75	270
Ptolemy Trench	25.3, 34.8	7.0	2	33	17	2.5	75	65	270
South Cretan Sea	24.8, 35.5	7.1	2	40	19	2.7	270	50	270
Karpathos I	27.1, 35.9	7.0	2	33	17	2.5	200	80	240
Rhodes	28.7, 36.4	7.3	3	50	23	3.2	328	73	71

*UBDF – Upper Border Depth of the Fault

4. RESULTS OF THE TSUNAMI SIMULATIONS

The tsunami initial condition for scenario WHA is presented in the upper panel of Fig. 4. The source is considered as thrust fault and it is placed almost parallel to the western Hellenic Subduction zone. This fault generated a sea bottom deformation characterized by high uplift near southwestern Crete and a subsidence near the northwestern coasts of Crete. The maximum positive and negative vertical deformations are 4.1 m and –1.6 m, respectively. The initial condition of scenario regarding the EHA thrust faulting source is presented in the upper panel of Fig. 4. The source, whose parameters are listed in Table 1, generated initial maximum and minimum sea water elevations of 3.3 m and –0.4 m, respectively. This scenario is associated with $M_w \sim 8.0$ and it is located offshore the southeastern coastline of Crete. The vertical displacements of the sea bottom for other modeled tsunamigenic sources are plotted in Fig. 4 (lower panel). South Cretan Sea tsunamigenic fault induced minimum water elevations –1.5 m, while Rhodes fault generated the maximum displacement of 1.5 m near the southwestern Turkish coast.

The propagation of the tsunami waves for all scenarios is presented as plots at 5, 20, 40 and 60 minutes intervals after the tsunami onset. The tsunami radiation pattern simulated for the two key events AD 365 and AD 1303 is illustrated in Fig. 5. The upper panel describing the tsunami propagation indicates that after only 5 minutes the waves have already attacked the southeastern coast of Crete. In 20 minutes the tsunami propagates northeast toward Karpathos and southwest toward the coasts of Crete. The Turkish and the Libyan coasts are reached by initially positive tsunami waves 40 minutes after the earthquake. One hour after the tsunami onset peninsula Peloponnese and the whole southern Aegean Sea is affected. The lower panel of Fig. 5 presents the tsunami radiation pattern simulated for AD 1303 event. The southwestern part of Crete, the islands Kythira and Gavdos are affected by the strong positive waves in 5 minutes after the earthquake. The propagation spreads in southwestern direction toward Libya and Ionian Sea. Most of the small islands north of Crete are attacked in 40 minutes. In one hour the eastern part of Mediterranean, including Alexandria and Cyprus is inundated. Both of the events are considered to be the largest historical tsunamis of tectonic origin in the region of Mediterranean. Tsunami radiation pattern modelled by other tsunamigenic sources is presented in Fig. 6 and Fig.7. Since the magnitude and the geometry of the six sources are smaller than the reconstructed events above, as expected, the tsunami waves are not so violent. The morphology beneath the southern Aegean Sea is very complex and therefore the propagation is slower.

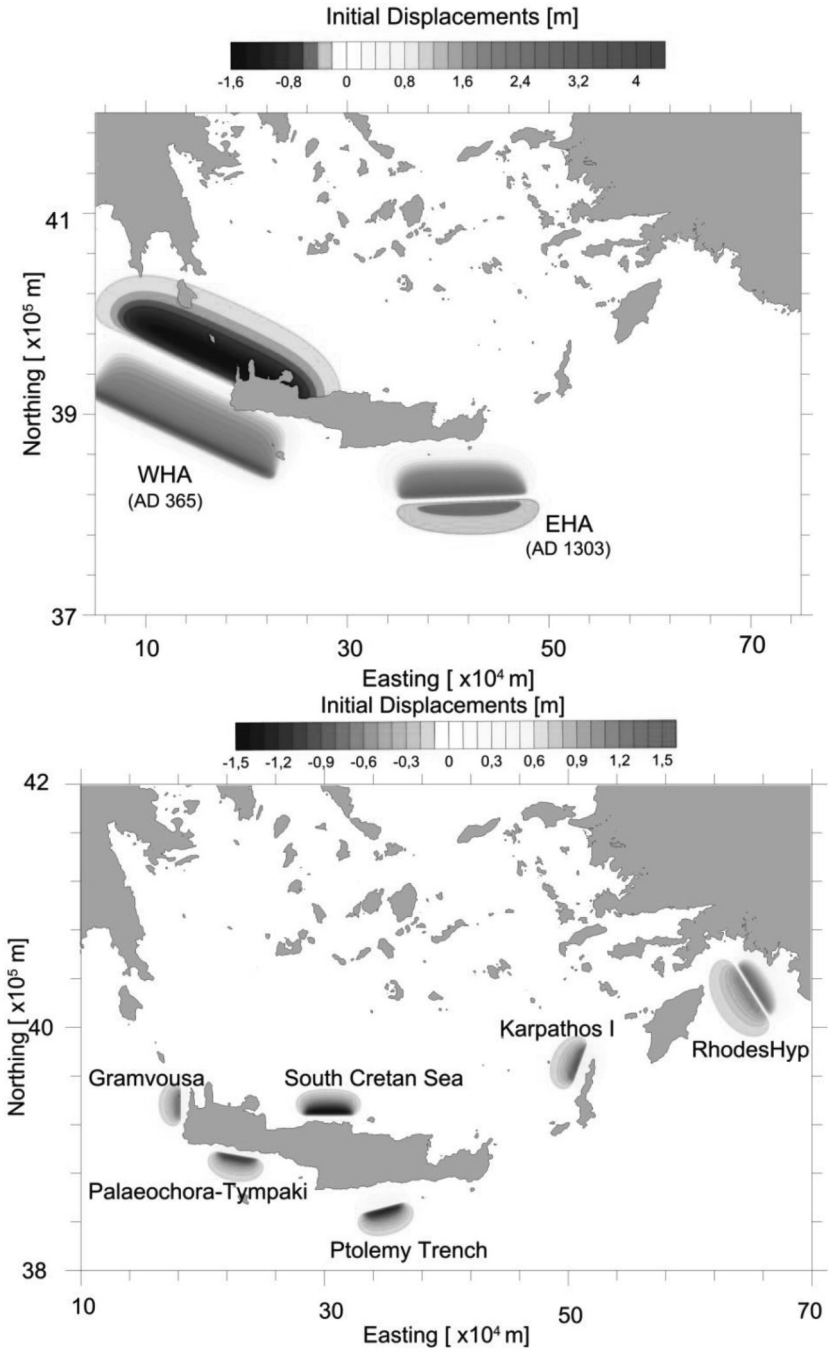

Fig. 4. Initial displacements (upper panel – WHA and EHA, lower panel – Gramvousa, Palaeochora-Tympaki, Ptolemy Trench, South Cretan Sea, Karpathos I and Rhodes)

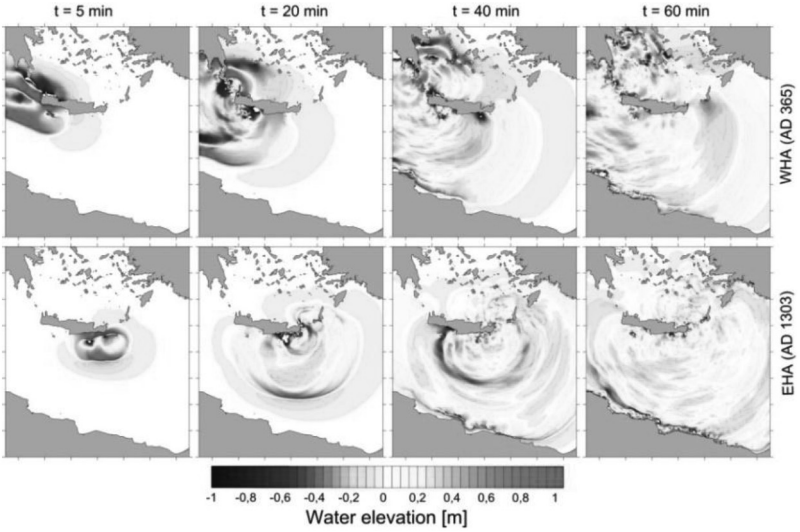

Fig. 5. Radiation pattern of the computed tsunami elevations for WHA and EHA

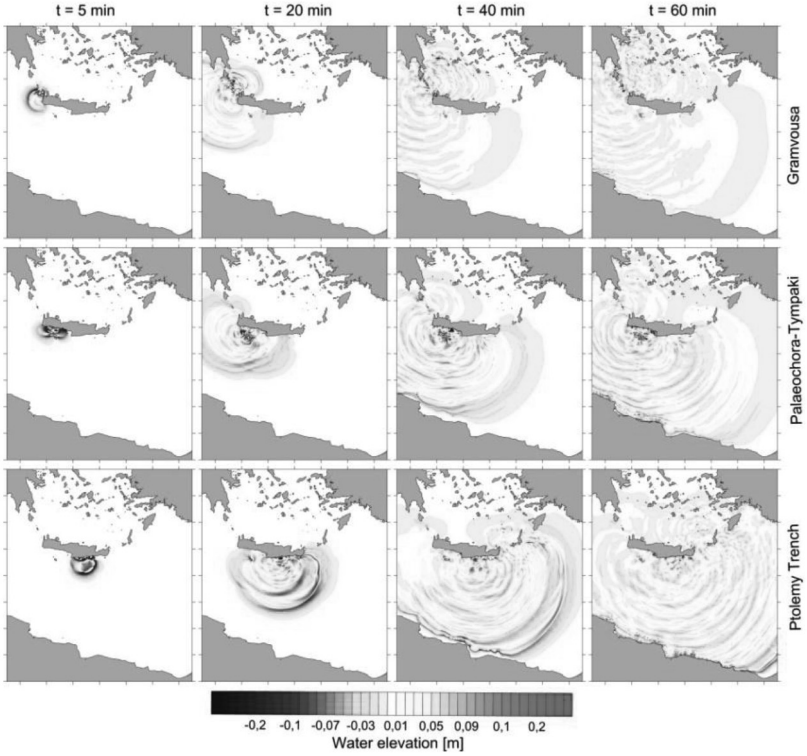

Fig. 6. Radiation pattern of the computed tsunami elevations for Gramvousa, Palaeochora-Tympaki and Ptolemy Trench

The effects can be considered as local, near the sources. Due to the large number of islands in the Aegean Sea, the tsunami waves diffract and this is clearly illustrated in both of the figures, and especially in the case of South Cretan Sea simulation (Fig. 7, upper panel). The propagation of the tsunami due to Rhodes source affects mostly the southwestern coast of Turkey, in particular the gulf of Fethiye and the whole Rhodes in less than 20 minutes after the earthquake.

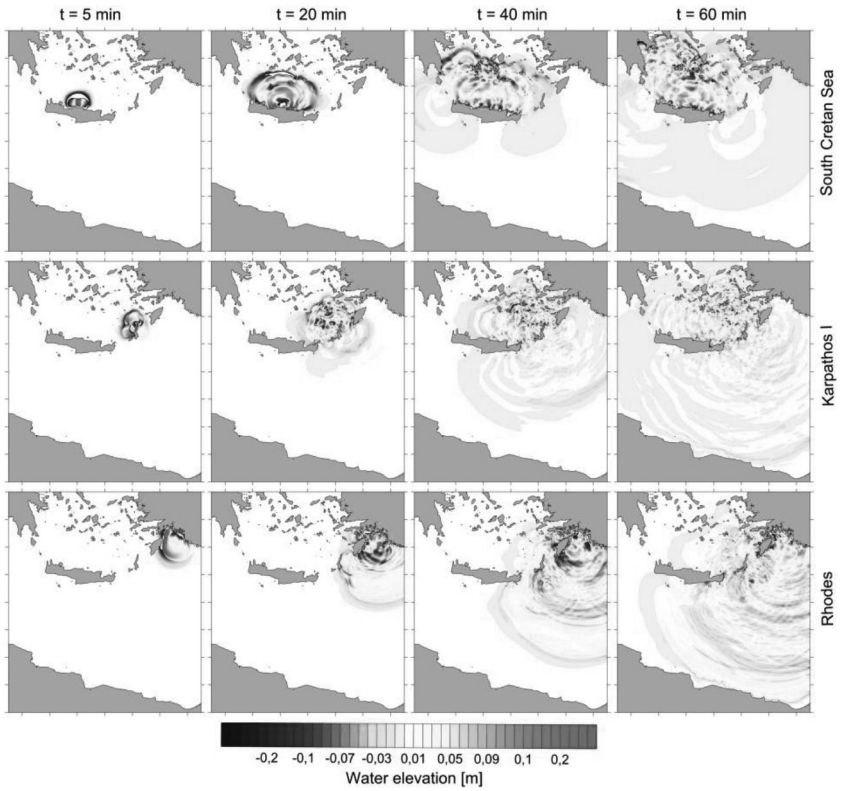

Fig. 7. Radiation pattern of the computed tsunami elevations for South Cretan Sea, Karpathos I and Rhodes

Fig. 8 and Fig. 9 show the maximum positive water elevation due to the events. The tsunami heights field can be interpreted as an indication of the released tsunami energy. Figures clearly illustrate the most affected coastal areas. Severe tsunami effects are expected on the west, south and east coast of Crete due to AD 365 and AD 1303 events. Large part of the tsunami energy computed for WHA propagates toward the western part of the Mediterranean, while EHA tsunamigenic source extend its energy to the south, reaching the coasts of Libya and Egypt and to the north attacking the island of Karpathos (Fig. 8).

As expected the maximum positive tsunami heights computed for the rest of the scenarios are smaller. The direction of the tsunami energy propagation strongly depends on the geometry of sources. Tsunami effects are expected in the region of whole Crete, southern Peloponnese, the islands north of Crete, Karpathos, Rhodes and southwestern part of the Turkish coast, including the cities Marmaris and Fethiye (Fig. 9).

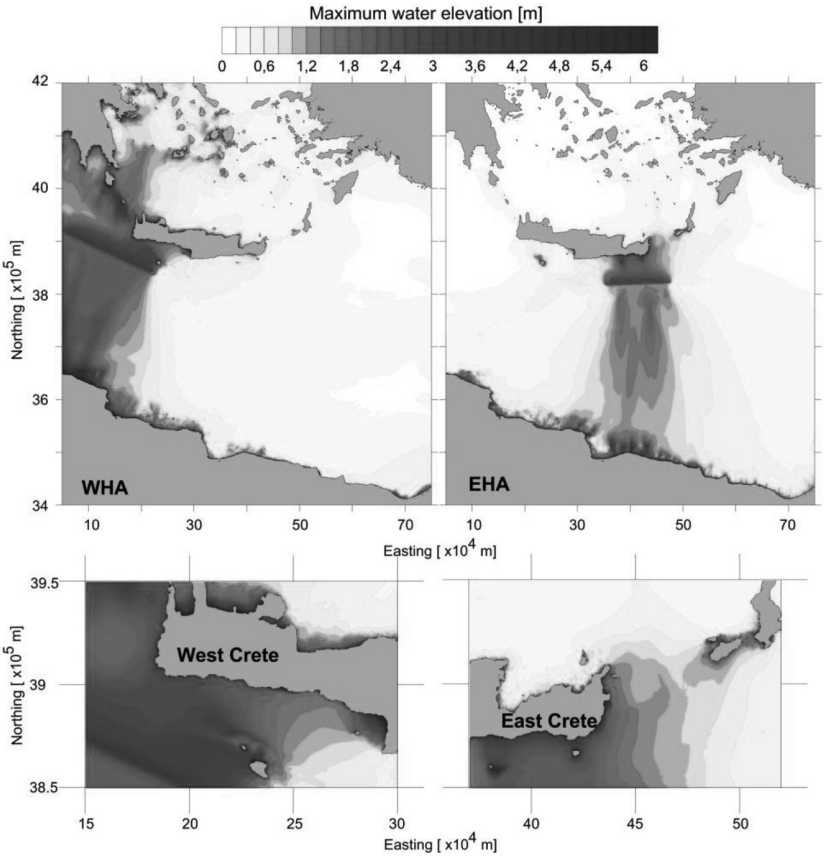

Fig. 8. Maximum positive tsunami wave heights computed for the WHA and EHA scenarios

The contribution of all modeled scenarios in southern Aegean Sea is presented in Fig 10. The colored areas represent the maximum tsunami wave heights. The figure shows the geographical distribution of the tsunami impact from studied events. It is evident that events like AD 365 (WHA) and AD 1303 (EHA) give the highest impact, but also Rhodes tsunamigenic zone must not be neglected, since the position of the source is very close to the coast and therefore the time for cities' evacuation like Fethiye is less than 10 minutes. South Cretan Sea source is the scenario contributing most to the impact of the islands in southern Aegean Sea.

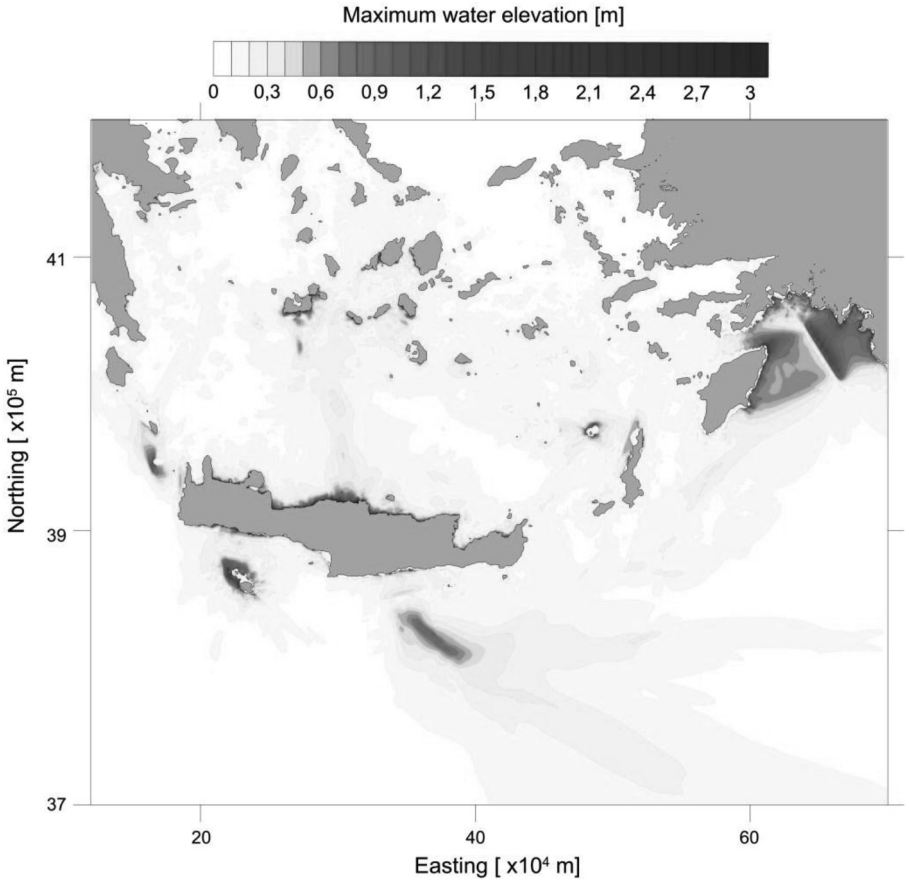

Fig. 9. Maximum positive tsunami wave heights computed for Gramvousa, Palaeochora-Tympaki, Ptolemy Trench, South Cretan Sea, Karpathos I and Rhodes scenarios

Synthetic mareograms in different locations are computed by the code. The mareograms reproduce the variations in the sea water elevation depending on the time elapsed from the earthquake onset. The position of considered mareograms is plotted in Fig. 11. Mareograms modeled for the scenario of South Cretan Sea tsunamigenic source are located in Santorini (Thera), Panormos and Heraklion and are presented in Fig. 12. The figure shows water level for 1 hour and 40 minutes after the earthquake occurrence.

Maximum modeled tsunami wave heights near Santorini are about 1.2 m (Fig. 12a), in Panormos are about 2.3 m (Fig. 12b) and in Heraklion the maximum water elevation is about 1.8 m (Fig. 12c).

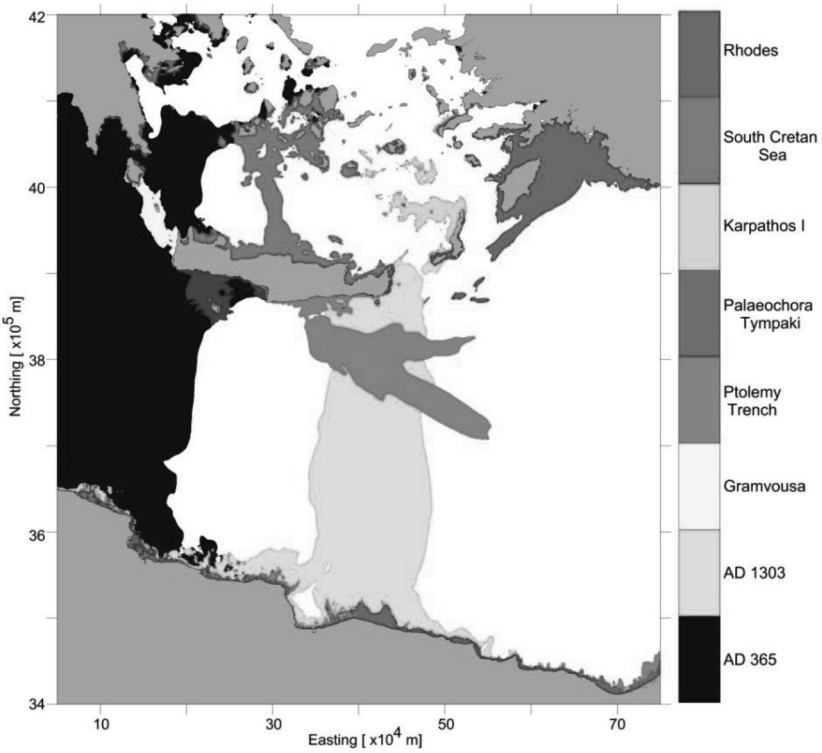

Fig. 10. Contribution given by all scenarios according to the computed tsunami wave heights

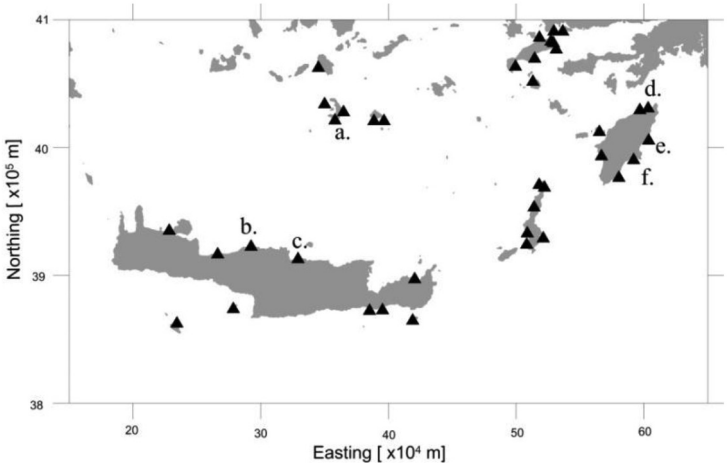

Fig. 11. Position of synthetic mareograms. The mareograms in labeled locations are shown in Figures 12 and 13

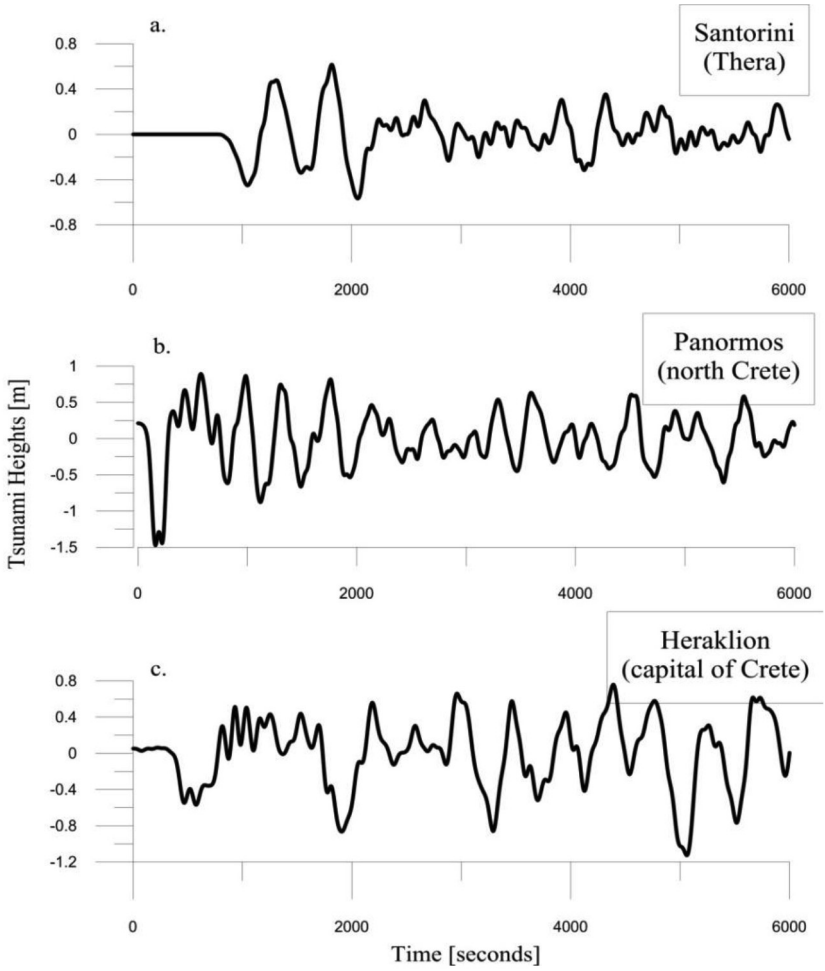

Fig. 12. Synthetic mareograms computed for scenario South Cretan Sea. Locations of mareograms are shown in Fig. 11

Synthetic mareograms calculated for the scenario of Rhodes tsunamigenic source are located in Rhodes, Stegna and Lardos and are illustrated in Fig. 13. Maximum modeled tsunami wave heights near Rhodes are about 2.5 m (Fig. 13d), in Stegna the water elevation is about 2.0 m (Fig. 13e) and in Lardos the maximum water amplitude is about 2.8 m (Fig. 13f). The first arrived wave is negative which corresponds to the initial displacements of the source. The eastern part of the island is the most affected due to Rhodes tsunamigenic fault. The period of the waves is much shorter than the period of the oscillations for scenario South Cretan Sea.

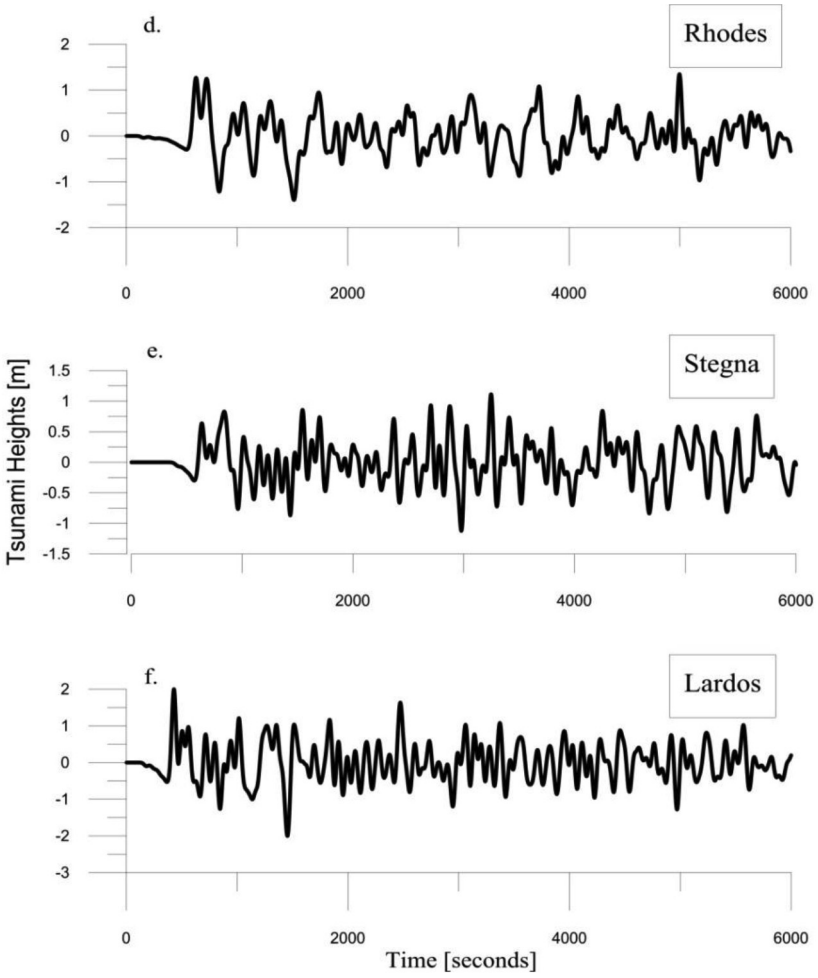

Fig. 13. Synthetic mareograms computed for scenario Rhodes.
Locations of mareograms are shown in Fig. 11

5. CONCLUSIONS

We examined scenarios of tsunami radiation pattern from eight seismic sources in the southern Aegean Sea. Based on numerical simulations the largest historically known tsunamis in the Mediterranean AD 365 and AD 1303 are well reconstructed. Most of the studied sources are situated close to the coasts which results in less time for evacuation. Crete, Rhodes, Karpathos and the southwestern part of the Turkish coast are at high risk of inundation due to tsunami waves.

Acknowledgements. The author thanks the Tsunami Research Team from University of Bologna, Department of Physics and Astronomy, Sector Geophysics, for suggestions and possibility to work with UBO-TSUFD.

REFERENCES

[1] International Seismological Centre. *On-line Bulletin*, http://www.isc.ac.uk, Internatl. Seismol. Cent., Thatcham, United Kingdom, 2015.
[2] National Geophysical Data Center / World Data Service (NGDC/WDS): Global Historical Tsunami Database. National Geophysical Data Center, NOAA. doi:10.7289/V5PN93H7.
[3] Shaw, B., N. Ambraseys, P. England, M. Floyd, G. Gorman, T. Higham, J. Jackson, J. Nocquet, C. Pain, M. Piggott. *Nature Geocsience*, 2008, **1**, 268.
[4] Papadopoulos, G. A., E. Gràcia, R. Urgeles, V. Sallares, P. M. De Martini, D. Pantosti, M. González, A. Yalciner, J. Mascle, D. Sakellariou, A. Salamon, S. Tinti, V. Karastathis, A. Fokaefs, A. Camerlenghi, T. Novikova, A. Papageorgiou. *Marine Geology*, 2014, **354**, 81.
[5] Tinti, S., A. Armigliato, G. Pagnoni, F. Zaniboni. *ISET Journal of Earthquake Technology*, 2005, **42**, 4, 171.
[6] Lorito, S., M. Tiberti, R. Basili, A. Piatanesi, G. Valensise. *Journal of Geophysical Research*, 2008, **113**, B01301.
[7] Yolsal-Cevikbilen, S., T. Taymaz. *Tectonophysics*, 2012, **536-537**, 61.
[8] Hamouda, A. *Journal of African Earth Sciences*, 2006, **44**, 37.
[9] Basili, R., G. Valensise, P. Vannoli, P. Burrato, U. Fracassi, S. Mariano, M.M. Tiberti, E. Boschi. *Tectonophysics*, 2008, **453**, 1, 20.
[10] Ebeling C., E. Okal, N. Kalligeris, C. Synolakis. *Tectonophysics*, 2012, **530-531**, 225.
[11] Yalciner, A. C., C. Ozer, H. Karakus, A. Zaytsev, I. Guler. In: *Proceedings of the 32nd International Conference Coastal Engineering, China,* 2010, https://doi.org/10.9753/icce.v32.management.10.
[12] Hanks, T., H. Kanamori. *Journal of Geophysical Research*, 1979, **84**, B5, 2348.
[13] Mai, M., G. Beroza. *Bull. of the Seis. Soc. of America*, 2000, **90**, 3, 604.
[14] Wells, D., K. Coppersmith. *Bull. of the Seis. Soc. of America*, 1994, **84**, 4, 974.
[15] Papadopoulos, G.A., E. Daskalaki, A. Fokaefs, N. Giraleas. *Natural Hazards and Earth System Sciences*, 2007, **7**, 57.
[16] Papadopoulos, G.A., A. Fokaefs. *ISET Journal of Earthquake Technology*, 2005, **42**, 4, 159.
[17] Yolsal, S. Source Mechanism Parameters and Slip Distributions of Crete-Cyprus Arcs, Dead Sea Transform Fault Earthquakes and Historical Tsunami Simulations. PhD Thesis, 523 pages, İstanbul Technical University, İstanbul, Turkey, November 2008.
[18] Guidoboni, E., A. Comastri. Catalogue of Earthquakes and Tsunamis in the Mediterranean area from the 11th to the 15th Century. INGV-SGA, p. 1037, Bologna, 2005.
[19] Ambraseys, N., R. Adam. The Seismicity of Egypt, Arabia and the Red Sea: A Historical Review, Cambridge University Press, Cambridge, UK, 1994.
[20] Okada, Y. *Bull. of the Seis. Soc. of America*, 1985, **75**, 4, 1135.
[21] Okada, Y. *Bull. of the Seis. Soc. of America*, 1992, **82**, 2, 1018.
[22] Tinti, S., R. Tonini. *Natural Hazards and Earth System Sciences*, 2013, **13**, 1759.
[23] Dimova, L., R. Raykova. *Ann. of Sofia Univ. "St. Kliment Ohridski", Faculty of Physics,* 2016, **109**, 24.
[24] British Oceanographic Data Centre. Gridded Bathymetry Data Sets. https://www.bodc.ac.uk/data/hosted_data_systems/gebco_gridded_bathymetry_data/.